Journal Name

ARTICLE TYPE

Cite this: DOI: 00.0000/xxxxxxxxxx

What Is "Many-Body" Dispersion and Should I Worry About It?

A. Otero-de-la-Roza,[a] Luc M. LeBlanc,[b] and Erin R. Johnson[b,*]

Received Date
Accepted Date

DOI: 00.0000/xxxxxxxxxx

Inclusion of dispersion effects in density-functional calculations is now standard practice in computational chemistry. In many dispersion models, the dispersion energy is written as a sum of pairwise atomic interactions consisting of a damped asymptotic expansion from perturbation theory. There has been much recent attention drawn to the importance of "many-body" dispersion effects, which by their name imply limitations with a pairwise atomic expansion. In this perspective, we clarify what is meant by many-body dispersion, as this term has previously referred to two very different physical phenomena, here classified as electronic and atomic many-body effects. Atomic many-body effects refer to the terms in the perturbation-theory expansion of the dispersion energy involving more than two atoms, the leading contribution being the Axilrod-Teller-Muto three-body term. Conversely, electronic many-body effects refer to changes in the dispersion coefficients of the pairwise terms induced by the atomic environment. Regardless of their nature, many-body effects cause pairwise non-additivity in the dispersion energy, such that the dispersion energy of a system does not equal the sum of the dispersion energies of its atomic pairs taken in isolation. A series of examples using the exchange-hole dipole moment (XDM) method are presented to assess the relative importance of electronic and atomic many-body effects on the dispersion energy. Electronic many-body effects can result in variation in the leading-order C_6 dispersion coefficients by as much as 50%; hence, their inclusion is critical for good performance of a pairwise asymptotic dispersion correction. Conversely, atomic many-body effects represent less than 1% of the total dispersion energy and are much less significant than higher-order (C_8 and C_{10}) pairwise terms. Their importance has been previously overestimated through empirical fitting, where they can offset underlying errors stemming either from neglect of higher-order pairwise terms or from the base density functional.

1 Introduction

London dispersion[1,2] is a weak type of van der Waals interaction, but it is also the main source of attraction between nonpolar chemical species. While the energetic stabilization from individual dispersion interactions is quite small, dispersion is ubiquitous in chemistry and, collectively, these interactions can determine adhesion[3] and friction,[4] surface adsorption,[5] conditions for phase changes,[6] stability of supramolecular complexes,[7] packing in molecular crystals,[8] and even the shapes of biomolecules.[9] However, despite the importance of dispersion, it has until relatively recently been neglected in density-functional theory (DFT),[10–12] which constitutes the most popular class of quantum-mechanical methods for computational studies spanning the fields of chemistry, biochemistry, and materials physics.

Conventional methods within DFT include only local and semilocal models of electron correlation, and hence do not include the highly non-local correlations responsible for dispersion. To correct for this shortcoming, many dispersion methods have been proposed over the past 15 years.[13–16] While explicitly nonlocal dispersion functionals have been developed,[17–21] and are quite popular in solid-state applications, their computational cost makes their use less than desirable for large systems. As a result, we will focus here on dispersion corrections where the dispersion energy is added to the energy obtained with some base density functional:

$$E_{\mathrm{DFT}} = E_{\mathrm{base}} + E_{\mathrm{disp}}, \tag{1}$$

where E_{base} contains a short-range local or semilocal correlation functional. Dispersion corrections of this type include Grimme's series of dispersion corrections (DFT-D2,[22] -D3,[23] and -D4[24]), the Tkatchenko-Scheffler (TS[25]) and many-body dispersion (MBD[26]) methods, and the exchange-hole dipole moment

[a] Departamento de Química Física y Analítica, Facultad de Química, Universidad de Oviedo, 33006 Oviedo, Spain
[b] Department of Chemistry, Dalhousie University, 6274 Coburg Road, PO Box 15000 Halifax, Nova Scotia, Canada B3H 4R2. E-mail: erin.johnson@dal.ca

(XDM[27,28]) method of Becke and Johnson.

The chemists' picture of dispersion involves an instantaneous dipole moment in one atom or molecule caused by fluctuations in the electron distribution interacting with an instantaneous dipole moment in a neighbouring atom or molecule.[1] Hence, we think of dispersion as a predominantly pairwise interaction. However, much recent attention has been given to "many-body" dispersion effects,[26] with claims of their importance for molecular crystals,[29] layered materials,[30] surface adsorption,[31] and in water-protein interactions.[32] To interpret these results, we must first ask ourselves what exactly in meant by "many-body" dispersion.

To understand many-body effects on the dispersion energy, we begin by considering its asymptotic perturbation-theory expansion.[2,33] In perturbation theory, we can write the (damped) dispersion energy as a sum of pairwise atomic terms:

$$E_{\text{disp}}^{(2)} = -\sum_{i<j}\left(\frac{C_{6,ij}f_6(R_{ij})}{R_{ij}^6} + \frac{C_{8,ij}f_8(R_{ij})}{R_{ij}^8} + \frac{C_{10,ij}f_{10}(R_{ij})}{R_{ij}^{10}} + \cdots\right), \tag{2}$$

where the sum runs over all pairs of atoms, i and j, the C_n's are the dispersion coefficients, and R_{ij} is the internuclear separation. The $f_n(R_{ij})$'s are damping functions that prevent divergence of the asymptotic expansion at small R_{ij}, and vanish in the asymptotic limit. Higher-order terms involving more than two atoms also contribute to the dispersion energy. The leading beyond-pairwise contribution is the Axilrod-Teller-Muto (ATM) term,[34,35] which involves a sum over atomic trimers corresponding to the interaction between three atomic dipoles:

$$E_{\text{ATM}}^{(3)} = \sum_{i<j<k}\frac{C_{9,ijk}\left[3\cos(\theta_i)\cos(\theta_j)\cos(\theta_k)+1\right]f_9(R_{ij},R_{jk},R_{ki})}{R_{ij}^3R_{jk}^3R_{ki}^3}, \tag{3}$$

and there are even-higher-order terms for tetramers, pentamers, etc.

We say that the dispersion energy is pairwise additive if it is equal to the sum of the dispersion energies of all atomic pairs in the system. In general, the dispersion energy is not pairwise additive because of many-body effects, of which we can identify two types. The first consists of non-additivity in the pairwise dispersion terms (Eq. 2) due to changes in the dispersion coefficients when going from a single atom to an atomic pair, and to the whole interacting system. This type of non-additivity is caused by electronic effects, mostly electron delocalization between the atom under consideration and the rest of the system, particularly those atoms directly bonded to it. Therefore, we refer to this source of non-additivity as electronic many-body effects. The second type of non-additivity arises from the inclusion of three-atom and higher-order terms in the dispersion energy (Eq. 3 is the leading term), which are absent if one considers atom pairs in isolation. These are atomic many-body effects.

Our definition of electronic and atomic many-body effects can be compared with Dobson's classification of dispersion interactions.[36] Dobson-A effects are changes in dispersion coefficients, relative to free-atom values, resulting from the immediate chemical environment (such as arising from hybridization and chemical bonding). This can be thought of as encompassing only nearest-neighbour interactions within a molecule or solid. Dobson-B effects concern changes in the pairwise dispersion coefficients arising from longer-range interactions, such as electron delocalization or electrostatic interactions with distant atoms, as well as three-body ATM terms. Finally, Dobson-C effects are due to interactions between extended conducting systems at the infinite-separation limit, which are not present in most chemical systems and are not considered here. From these definitions, atomic many-body effects are thus only one aspect of the larger class of Dobson-B interactions, while electronic many-body effects include all of Dobson-A and some Dobson-B dispersion contributions. Hence, with the electronic versus atomic classification, it is possible to quantify how much each many-body effect contributes to the total dispersion energy, whereas this is not possible in Dobson's classification because the immediate chemical environment of an atom cannot be precisely defined.

Electronic many-body effects are typically accounted for in classical force fields,[37–39] and in early dispersion corrections,[40–43] through atom typing. Here, atoms of a particular element will be assigned set dispersion coefficients based on the bonding connectivity. In DFT-based dispersion corrections, these effects are included (to varying extents) by how the dispersion coefficients are obtained. The Grimme dispersion corrections have their roots in atom typing,[22] and the coefficients primarily depend on the coordination number of an atom.[23] For the TS correction,[25] the C_6 coefficients are obtained by a scaling of the free-atom values based on atomic polarizabilities, which are in turn approximated as being directly proportional to the atomic volumes.[44–46] The XDM and MBD models have more sophisticated means of obtaining the dispersion coefficients and will be discussed in the following sections. Within this work, we will focus on the XDM dispersion method, which has been shown to give consistent, excellent performance for molecular complexes,[47–50] molecular crystals,[51–55] metal surfaces,[56–58] and layered materials,[47,59] without any modification or re-fitting.

Previous works have investigated the effect of the chemical environment on the XDM C_6 dispersion coefficients in molecules,[60–62] in layered materials,[28,59] and for metal atoms in bulk solids or at surfaces.[28,56–58] In this work, we focus on the more subtle changes in dispersion coefficients resulting from neighbouring, weakly interacting atoms or molecules. The results highlight the importance of electronic many-body effects in modeling dispersion. Conversely, we simultaneously demonstrate that atomic many-body effects are much smaller in magnitude, and can be safely neglected in most applications. It is shown that the magnified role of the ATM term in other works is a result of empirical parameterization of the three-body damping function, allowing excessive repulsion from the C_9 term to offset excessive attraction from neglect of higher-order pairwise terms (C_8 and C_{10}) or from the base density functional.

2 The XDM Dispersion Model

In the XDM model, which will be used throughout this perspective, the dispersion coefficients are functions of the electron density (ρ), its derivatives ($\nabla\rho$ and $\nabla^2\rho$), and the kinetic-energy density (τ). The leading-order pairwise homoatomic dispersion coef-

ficients are

$$C_{6,ii}^{\mathrm{XDM}} = \frac{1}{2}\alpha_i \langle d_X^2 \rangle_i. \tag{4}$$

Here, the atomic polarizability is

$$\alpha_i = \left(\frac{V_i}{V_i^{\mathrm{free}}} \right) \alpha_i^{\mathrm{free}}, \tag{5}$$

which is proportional to the ratio of in-molecule and in-vacuo (free) atomic volumes, with $V_i = \langle r^3 \rangle_i = \int w_i(\mathbf{r}) \rho(\mathbf{r}) r^3 d\mathbf{r}$. $\langle d_X^2 \rangle_i$ is the exchange-hole dipole moment integral for atom i,

$$\langle d_X^2 \rangle_i = \int w_i(\mathbf{r}) \rho(\mathbf{r}) d_X^2 d\mathbf{r}, \tag{6}$$

and the w_i's are atomic partitioning weights.[63] Similarly, the C_9 triple-dipole term can also be evaluated in terms of the dipole moment integrals and polarizabilities.[64] For a homoatomic trimer, the C_9 coefficient is

$$C_{9,ii}^{\mathrm{XDM}} = \frac{3}{8}\alpha_i^2 \langle d_X^2 \rangle_i. \tag{7}$$

Higher-order pairwise dispersion terms, including C_8 and C_{10}, can be evaluated using higher-order multipole moments (quadrupole and octopole) of the exchange hole.[27,45] The 2ℓ-pole moments are

$$\langle M_\ell^2 \rangle_i = \int w_i(\mathbf{r}) \rho(\mathbf{r}) \left[r^\ell - (r - d_X)^\ell \right]^2 d\mathbf{r}. \tag{8}$$

General formulae for the heteroatomic C_6, C_8, C_{10}, and C_9 dispersion coefficients are presented elsewhere.[28,64]

The dipole and higher-order multipole moments in Eqns. 6 and 8 can be evaluated using the exact exchange hole,

$$\boldsymbol{d}_X(\boldsymbol{r}) = \left[\frac{1}{\rho(\boldsymbol{r})} \sum_{ij} \psi_i(\boldsymbol{r}) \psi_j(\boldsymbol{r}) \int \boldsymbol{r'} \psi_i(\boldsymbol{r'}) \psi_j(\boldsymbol{r'}) d\boldsymbol{r'} \right] - \boldsymbol{r}, \tag{9}$$

but in practise they are usually computed semi-locally as a function of the electron density and its derivatives at $\boldsymbol{r}$ using the Becke-Roussel (BR) model.[65,66] While the exact formalism is more accurate in free atoms,[45] the BR model is more realistic for atoms in molecules or solids since it implicitly models a localized hole including both exchange and non-dynamical correction effects.[67]

The BR model approximates the exchange hole as an off-center exponential function centered some distance d_X from the reference electron.[66] This model is exact for the H atom,[65] where the exchange hole is simply the negative of the electron density distribution, which takes the form of an exponential function centered at the nucleus. For many-electron atoms, the center of the hole will be displaced slightly away from the nucleus, closer to the reference point,[27] as shown in Figure 1. Nevertheless, for reference points far from the nucleus, the hole remains centered on the atom, so more diffuse density distributions typically have a larger proportion of points with both significant density and large exchange-hole dipole moments, resulting is larger moment integrals. Conversely, more compact density distributions tend to have smaller moment integrals. This connection is key to understanding the reduction in moment integrals and C_6 coefficients previously seen in going from a free atom to an atom at a surface or in a bulk metal.[56] In the bulk, there are no reference points far from any atomic centre, resulting in roughly a 50% decrease in the moment integrals compared to the free-atom values.

Fig. 1 Sketch of the BR exchange hole in a many-electron atom; the center of the hole is displaced away from the nucleus and towards the reference electron.

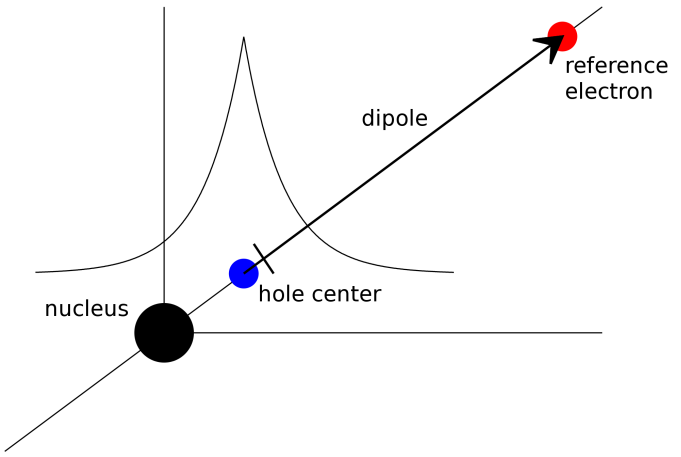

3 A Model System: Drude Oscillators

Before proceeding to the discussion of atomic and molecular systems, we first consider a simple analytical model that underlies several of the DFT dispersion corrections,[25,26] involving the interaction between Drude oscillators. A Drude oscillator is a model of the H atom, which consists of positive and negative point charges of ± 1 a.u. separated by a harmonic spring. The vibrational frequency of the oscillator is

$$\nu = \frac{1}{2\pi}\sqrt{\frac{k}{\mu}}, \tag{10}$$

where μ is the reduced mass. The polarizability of the system is determined by the spring constant, k,

$$\alpha = \frac{e^2}{k}, \tag{11}$$

where $e = 1$ a.u. is the electron charge. The homoatomic dispersion coefficient of an isolated Drude oscillator can be obtained exactly[68]:

$$C_6 = \frac{3}{4}\alpha^2 h\nu. \tag{12}$$

This result is reproduced exactly by the XDM model. To evaluate the dipole-moment integral, we use the wavefunction for the ground state of a 3D harmonic oscillator:

$$\psi = \left(\frac{\mu k}{\pi^2 \hbar^2} \right)^{3/4} \exp\left[-\frac{1}{2} \left(\frac{\mu k}{\hbar^2} \right)^{1/2} \mathbf{r}^2 \right]. \tag{13}$$

The dipole moment is simply $d_X = r$, so the density-weighted integral gives

$$\langle d_X^2 \rangle = \frac{3}{2}\frac{e^2}{k}\hbar\sqrt{\frac{k}{\mu}} = \frac{3}{2}\alpha h\nu, \tag{14}$$

using the definition of α and ν. Thus, taking the dispersion coefficient as one-half the product of the moment integral and polarizability (Eqn. 4), this reduces to the exact result of Eqn. 12.

For multiple interacting Drude oscillators, collective oscillations give rise to the non-additive ATM term. However, it is also possible that the presence of neighbouring oscillators affect the polarizabilities, and hence the C_6 dispersion coefficients. It is this latter phenomenon that is the source of electronic many-body effects. For a system comprised of many interacting atoms, each treated as a Drude oscillator, self-consistent solution is needed to obtain each polarizability in the presence of all the other atoms. Indeed, it is this picture that is at the heart of the MBD dispersion method.[26]

In MBD, an initial set of dispersion coefficients is obtained from the TS model[25] as

$$C_{6,ii}^{\mathrm{TS}} = \left(\frac{\alpha_i}{\alpha_i^{\mathrm{free}}}\right)^2 C_{6,ii}^{\mathrm{free}} = \left(\frac{V_i}{V_i^{\mathrm{free}}}\right)^2 C_{6,ii}^{\mathrm{free}}, \qquad (15)$$

where the volume scaling is expected to capture Dobson-A effects[36] and (often incorrectly[56,59]) account for the majority of the differences from the free-atom values. Next, the self-consistent screening formalism (SCS)[26] is used to model longer-range non-additivities in the atomic polarizabilities and dispersion coefficients (Dobson-B effects[36]). Here, the atoms comprising the system are each treated as a spherical quantum harmonic oscillator with a Gaussian density, analogous to the square of Eqn 13. The initial polarizabilities of the oscillators are taken from the TS model. The individual oscillators are then allowed to interact electrostatically until a self-consistent set of polarizabilities is obtained. These polarizabilities are used to calculate the SCS dispersion coefficients.

Finally, a coupled fluctuating dipole model Hamiltonian corresponding to the SCS model is constructed using the self-consistent frequencies and polarizabilities. This model involves the sum of kinetic and potential energies of the individual oscillators, as well as an empirically damped dipole-dipole Coulomb interaction energy. Diagonalization of the numerically solvable model Hamiltonian yields the MBD dispersion energy, taken as the difference between the ground-state energies of the Hamiltonians with interacting and non-interacting oscillators. This definition allows the quantification of Dobson-B effects[36] as the difference between the MBD and TS dispersion energies. However, it should be stressed that this interpretation of many-body effects is fundamentally tied to the details of the TS and MBD methods and, specifically, to the approximate harmonic-oscillator model used in the computation of the corresponding dispersion energies. In contrast, our definition of atomic many-body and electronic many-body effects can be generalized to any asymptotic dispersion correction. For analysis of electronic many-body effects, it is informative to consider the changes between free-atomic, TS, and MBD C_6 dispersion coefficients. Interestingly, MBD and XDM results are in excellent agreement for the changes in dispersion coefficients between free atoms and bulk metals,[56] as well as for compression of bilayer graphene.[59]

Fig. 2 Ratio of C_6 dispersion coefficients for homoatomic dimers and trimers, relative to free-atom values.

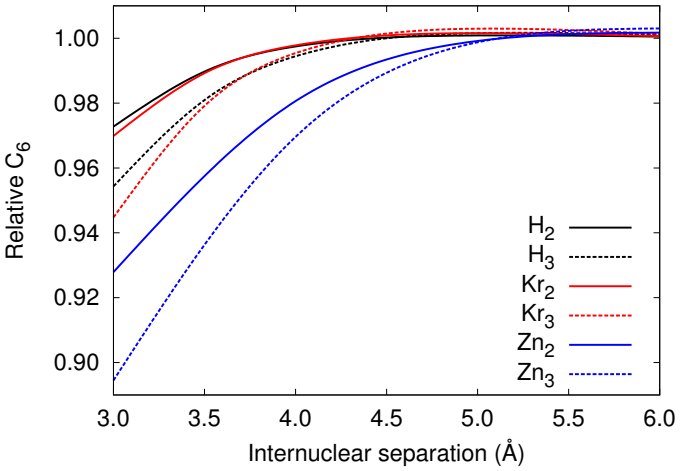

4 Electronic Many-Body Effects in Small Model Systems

In this section we apply the XDM model to several simple model systems in order to illustrate atomic many-body effects (i.e. the non-additivity in C_6 dispersion coefficients with changes in chemical environment) resulting from the introduction of neighbouring atoms, molecules, or point charges. These tests will primarily employ free atoms, as well as weakly interacting van der Waals complexes consisting of atomic dimers and trimers. The complexes are formed from spin-polarized H atoms, as well as the closed-shell Kr and Zn atoms, which were chosen to include only monoatomic species, covering a range of atomic sizes and polarizabilities. In this section, all calculations were performed with the Gaussian 09[69] and postg[70] programs using the PBE0 functional[71] and the aug-cc-pVTZ basis set, following our previous work on comparison of XDM and force-field dispersion coefficients.[61,62] The BJ damping-function parameters were set to their canonical values ($a_1 = 0.4186$ and $a_2 = 2.6791$ Å).[48,72]

Figure 2 shows the change in the computed XDM C_6 dispersion coefficients, expressed as a fraction of the free-atom values for the H, Kr, and Zn homo-atomic dimers and trimers (D_{3h} symmetry) at a range of internuclear separations. The results are reminiscent of our previous finding for the variation of the carbon C_6 coefficient in graphite with respect to interlayer separation,[59] and the decreases in C_6 at short internuclear separations are due to the behaviour of the moment integrals. This occurs because increasing Pauli repulsion with neighbouring atoms upon compression of the dimer or trimer causes the atomic densities to become more compact, decreasing the moment integrals. Compared to the change in moments, variation in the atomic polarizabilities with compression is minor. For the smallest (3 Å) separation considered, atomic polarizabilities decrease by only 0.2-1% relative to the free-atom values, while the decrease in C_6 coefficients (3-11%) is roughly a factor of 10 larger, confirming that reduction of the moment integrals is almost exclusively responsible for the decrease in C_6.

Next, we consider the case of interactions of the same three monoatomic species (H, Kr, and Zn) with ions, represented by

Fig. 3 Ratio of C_6 dispersion coefficients, relative to free-atom values, as a function of the distance to a point charge of ± 1 a.u. (solid=positive, dashed=negative).

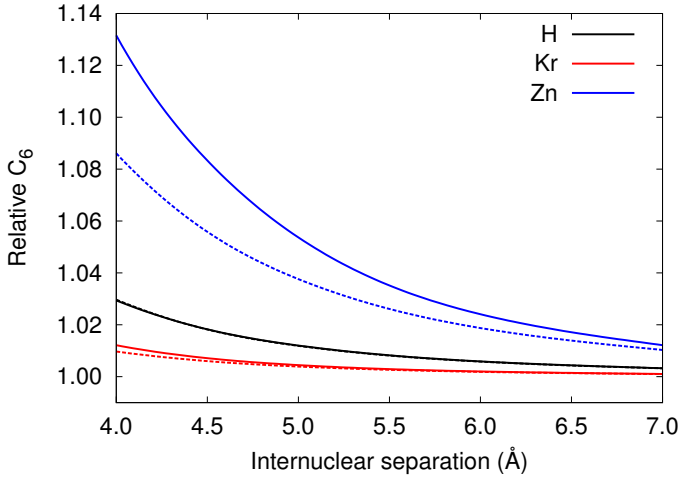

point charges. Figure 3 shows the change in the computed XDM C_6 dispersion coefficients, expressed as a fraction of the free-atom values, as a function of the distance to a point charge of ± 1 a.u. The results are contrary to those for the vdW dimers and trimers, with the presence of a point charge resulting in an increase in C_6. The increases in C_6 follow the trend Kr<H<Zn, with larger changes in C_6 occurring for positive point charges. In this case, the change in polarizability (0.5-8.5%) is comparable to, or larger than, the change in moment integrals (0.6-4.7%). The presence of the point charge serves to polarize the electron density, increasing the atomic volume and polarizability. Concurrently, the polarization results in an increased number of reference points far from the nucleus with appreciable electron density, which increases the moment integrals. Since the moment integrals are dominated by contributions from the most diffuse orbitals, and hence the most weakly bound electrons, the trend of Kr<H<Zn follows the computed PBE0 HOMO energies ($-10.8 < -9.1 < -6.5$ eV) or the negative of the free-atom ionization potentials ($-14.0 < -13.6 < -9.4$ eV[73]).

We now consider hydrogen bonding in the water dimer as an intermediate and more realistic case between the last two: a dimer with strong electrostatic interaction between the monomers. The homomolecular C_6 of water, which is a sum over all possible atomic pairs for a water-water interaction, is

$$C_{6,\mathrm{water}} = C_{6,\mathrm{O-O}} + 4C_{6,\mathrm{O-H}} + 4C_{6,\mathrm{H-H}}. \qquad (16)$$

To quantify the contributions to the molecular C_6, the moment integral for water is also a simple sum over atomic contributions, and the polarizability is determined as $\alpha = 2C_6/\langle d_X^2 \rangle$. Results for the homomolecular C_6 are shown in Table 1 for an isolated water molecule, the water dimer, and the chair conformation of the water hexamer (S_6 symmetry). For the dimer, the C_6 for the H-bond donor and acceptor are reported separately. In the hexamer, all six molecules are symmetry equivalent and each act as both a donor and acceptor.

The data in Table 1 show that hydrogen bonding can have a

Table 1 XDM homomolecular C_6 dispersion coefficients for an isolated water monomer, as well as the hydrogen-bonded dimer and the chair conformation of the hexamer (S_6 symmetry). Contributions from the moment integrals and polarizabilities are also shown. All quantities are in atomic units.

System	Molecular C_6	$\langle d_X^2 \rangle$	α
Monomer	44.02	8.30	10.61
Dimer, donor	49.92	8.64	11.56
Dimer, acceptor	39.67	7.63	10.40
Hexamer	42.43	7.81	10.87

substantial effect on C_6, with changes again on the order of 10%. Consistent with the point-charge results, both the moment integrals and polarizabilities contribute to the changes in C_6 for water, although the polarizability term has a larger effect for the H-bond donor, while the moment integral has a larger effect for the H-bond acceptor. In the H-bond donor, there is increased polarization, with a more positive hydrogen charge and more negative oxygen charge than in the isolated water, resulting in a substantial increase in C_6. Conversely, in the acceptor, the formation of the H-bond results in compaction of the oxygen lone pairs, primarily reducing the moment integrals and dispersion coefficient. In the hexamer, where all molecules act as both H-bond donors and acceptors, the effects partially offset, with increased polarization increasing the α term and Pauli repulsion decreasing the $\langle d_X^2 \rangle$ term; the latter effect is larger, resulting in a net decrease in C_6.

As an aside, considering a calculation on an isolated water molecule with aqueous PCM solvent[74] results in a slight increase in C_6, up to 44.4 a.u. This is because the continuum solvent results in a slight increase in the polarizability of water, but the overall contribution from the moment integrals is effectively constant as the continuum model does not account for the effects of Pauli repulsion with surrounding water molecules in solution.

Additionally, the choice of density functional can affect the calculated dispersion coefficients, particularly if delocalization error[75–78] is present, as it will increase the extent of polarization and charge transfer between interacting molecules. While the results in Table 1 used the PBE0 hybrid functional,[71] the PBE[79] GGA gives marginally larger dispersion coefficients of 45.24 and 43.06 a.u. for water and water hexamer, respectively. For the water dimer, the two interacting water molecules are inequivalent and there is a slight charge transfer (0.008 e^- with PBE0 and 0.011 e^- with PBE), providing a greater potential for delocalization error to affect the electron density distribution. This results in PBE magnifying the changes in C_6 relative to the isolated water molecule, yielding values of 51.41 and 38.25 a.u. for the H-bond donor and acceptor, respectively.

For comparison, changes in C_6 with atomic environment are much more significant going from free atoms to atoms in molecules[60] or bulk solids,[56,59] where decreases in excess of 50% are common. Nevertheless, the results here demonstrate that even non-bonded contacts in vdW clusters, or hydrogen bonding, can result in variations of atomic and molecular C_6 coefficients on the order of 10%. Thus, even in weakly interacting systems, elec-

Table 2 Undamped XDM dispersion energies for atomic dimers and D_{3h} trimers, at internuclear separations of 6 Å, expressed as a percentage of total dispersion energy ($E_6+E_8+E_{10}+E_9$).

System	E_6	E_8	E_{10}	E_9
H_2	80.1	15.7	4.2	—
H_3	80.0	15.7	4.2	0.1
Kr_2	69.4	23.3	7.3	—
Kr_3	69.2	23.2	7.3	0.3
Zn_2	63.6	25.2	11.2	—
Zn_3	63.3	25.0	11.1	0.6

tronic many-body effects can be significant and should be taken into account in DFT dispersion corrections.

5 Higher-Order Pairwise Terms and Atomic Many-Body Effects

We now consider the importance of atomic many-body effects. For this, we return to the H, Kr, and Zn atomic dimers and trimers to assess the relative magnitude of the various pairwise terms compared to the leading atomic three-body contribution – the ATM term. To avoid dependence on the choice of damping function, we consider the undamped dispersion energies at a relatively large internuclear separation (6 Å), well beyond the sum of van der Waals radii but still illustrative of typical interaction distances in chemical systems.

Table 2 shows the relative contributions of the pairwise C_6, C_8, and C_{10}, and the 3-body C_9 term, to the total dispersion energy. The atomic size and dispersion coefficients follow the order H<Kr<Zn, and thus the percent contributions from the higher-order terms follow this same trend. At constant internuclear separation, the larger the atomic size, the more important higher-order dispersion-energy terms become, which makes sense because the interatomic distance is relatively farther away from the infinite-separation limit for heavier atoms. Indeed, this is why the Becke-Johnson damping function was designed to damp higher-order terms faster than C_6.[80]

Overall the contribution to the total dispersion energy follows the expected trend of $E_6 > E_8 > E_{10}$, with $E_9 \ll E_{10}$, in agreement with previous results for molecular systems.[64,81] The results demonstrate that, for atomic trimers, the C_9 term is very much smaller than the C_{10} term and contributes less than 1% to the total dispersion energy. Indeed, higher-order pairwise terms beyond C_{10} would have larger contributions to the dispersion energy than the C_9 triple-dipole term, but are not included in the XDM dispersion energy since the statistics for dimer binding energies do not improve appreciably with their inclusion.[64] Thus, initial findings for small model systems lead to the conclusion that the 3-body ATM term is negligible.

6 Importance of Higher-Order Pairwise Terms for Molecular Systems

We now investigate the effect of including higher-order pairwise (C_8 and C_{10}) dispersion terms on binding energies of molecular dimers and lattice energies of molecular crystals. As a numerical experiment, the BJ damping function[80] was parameterized by truncating the XDM dispersion energy at the C_6 or C_8 terms. Additionally, a multiplicative factor was also introduced to scale the highest-order pairwise dispersion term, as in the D3 model.[23,82] As usual with XDM, the damping parameters were fit to minimize the root-mean-square percent (RMSP) error for the Kannemann-Becke set of 49 molecular dimers (KB49).[47,83] The performance of the resulting XDM variants was then assessed for the X23[29,51] set of lattice energies of 23 molecular crystals. The results are shown in Table 3.

All calculations on the KB49 and X23 sets were performed using plane-wave basis sets and the projector augmented wave (PAW) method,[84] with the Quantum ESPRESSO program.[85] The wavefunction and density cut-offs were 80 and 800 Ry, respectively. Both the PBE[79] and B86bPBE[79,86] density functionals were considered. The former is more popular in the literature for use with other dispersion corrections, while the latter is our functional of choice to pair with XDM due to its desirable large-gradient behaviour.[28,87–90] The KB49 computations kept the molecules and dimers fixed at their reference geometries[83] and used cubic supercells with cell lengths of 40 Bohr. For the X23 crystals, the geometries were obtained using our usual XDM implementation (including C_6, C_8, and C_{10} terms) with a $4\times4\times4$ k-point grid and convergence thresholds of 10^{-5} Ry in the energy and 10^{-4} Ry/bohr in the forces. The lattice energies were then evaluated with the various dispersion energy terms at the resulting geometries.

Looking first at the results without scaling in Table 3, it is clear that the C_6 term alone provides insufficient dispersion stabilization, resulting in underbinding of both the molecular dimers and the molecular crystals. Adding the C_8 term results in a large improvement in performance for both data sets. Indeed, during the development of XDM, the C_8 term was found to be essential for an accurate description of π-stacking.[80] Later results for supermolecular complexes[92] further highlighted the role of the C_8 and C_{10} terms. Returning to Table 3, adding the C_{10} term as well results in further modest improvement. There remains some systematic underbinding of the X23, particularly with the PBE base functional. This has been previously explained by the tendency of GGAs in general, and of PBE in particular because of its enhancement factor,[87–90] to overbind hydrogen bonds.[93,94] Thus, fitting results in excessive damping of the dispersion energy. Nevertheless, our favoured B86bPBE-XDM functional, with C_8 and C_{10}, gives good performance for both sets. In particular, the MAE of 0.86 kcal/mol for the X23 set is considerably lower than results obtained with other XDM-corrected GGAs and with other dispersion corrections.[29]

Inclusion of only the C_6 term with multiplicative scaling demonstrates a pitfall of empirical dispersion corrections. For molecular dimers, the C_6 term can be roughly doubled to augment the dispersion binding, giving KB49 error statistics that are even better than those obtained with unscaled C_6, C_8, and C_{10} terms. However, this results in massive overbinding for the X23 molecular crystals. Attempting to capture higher-order dispersion contributions with a scaled C_6 terms results in too slow an asymptotic decay in the dispersion energy, overestimating the stabilization from dispersion interactions with molecules beyond nearest

Table 3 Optimum XDM damping function parameters and resulting performance on the KB49 and X23 benchmarks for various combinations of dispersion-energy terms.[91] An "×" indicates an unscaled term and "s" indicates multiplicative scaling, with scaling parameter given in the s column. All errors are in units of kcal/mol (MAE, ME) or % (MAPE). MAE: mean absolute error; MAPE: mean absolute percent error; ME: mean error, a negative value indicates underbinding.

Pairwise Terms			Fit Parameters			KB49		X23	
C_6	C_8	C_{10}	a_1	a_2 (Å)	s	MAE	MAPE	MAE	ME
PBE-XDM									
×			0.4310	1.3059	–	0.754	19.7	1.73	-1.30
×	×		0.1786	2.9656	–	0.539	15.5	1.23	-0.90
×	×	×	0.3414	2.7242	–	0.500	14.2	1.12	-0.77
s			0.0106	3.9474	2.3191	0.4690	13.2	1.65	1.45
×	s		0.4125	2.8534	3.1090	0.483	13.3	0.89	-0.10
B86bPBE-XDM									
×			0.1133	1.8834	–	0.830	22.1	1.97	-1.59
×	×		0.4642	1.7092	–	0.483	13.7	0.94	-0.38
×	×	×	0.6632	1.4302	–	0.410	11.7	0.86	-0.26
s			0.3300	2.4391	2.0852	0.381	10.8	1.78	1.61
×	s		0.6897	1.5655	2.4615	0.395	10.9	0.84	0.08

Fig. 4 Potential energy surfaces for graphite exfoliation computed using the B86bPBE functional with the various dispersion corrections shown in Table 3. A reference QMC result[96] for the minimum-energy point is shown for comparison.

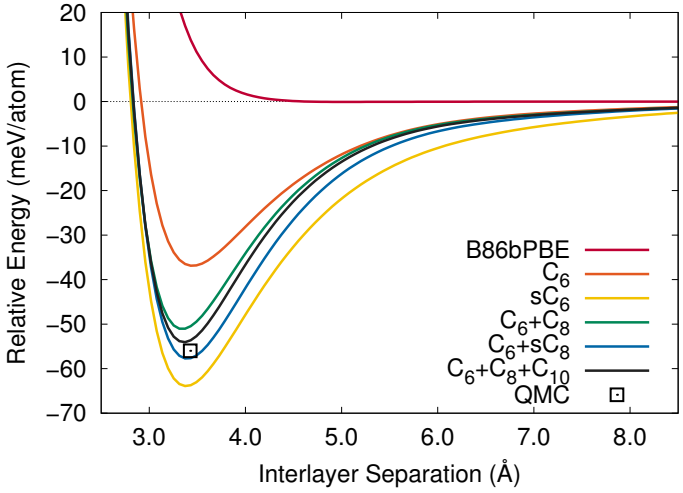

neighbours in the lattice. In the past, this has been suspected to affect both the TS dispersion model[51] and classical force fields,[61] and the results in Table 3 provide a concrete demonstration of the critical importance of C_8 for molecular crystals.

Finally, the combination of an unscaled C_6 and a C_8 dispersion energy scaled by a factor of 2.5–3 results in excellent performance for both the KB49 and X23, slightly better than what is obtained with unscaled C_6, C_8, and C_{10} terms. This is consistent with the success of the D3BJ dispersion method,[23,82,95] which also uses this combination of unscaled C_6 and scaled C_8. However, given that the resulting reduction of errors is small (particularly with B86bPBE) and the scaling of the C_8 is unphysically large, we prefer the less-empirical conventional XDM form with unscaled C_6, C_8, and C_{10} terms.

As an illustration of their differing behaviour at both short and long range, the various XDM-based dispersion corrections from Table 3 were used to compute potential energy surfaces for graphite exfoliation. The results are shown in Figure 4. These calculations used a $12 \times 12 \times 4$ k-point grid, wavefunction and density cutoffs of 80 and 800 Ry, respectively, and a cold smearing parameter of 0.001 Ry. The result with the B86bPBE base density functional is repulsive along the full PES, as expected. Additionally, as demonstrated previously,[16,47] the canonical XDM result ($C_6 + C_8 + C_{10}$) is in excellent agreement with Quantum Monte Carlo (QMC) reference data.[96]

Figure 4 shows that using the leading-order C_6 dispersion-energy term only results in substantial underbinding of the graphite layers, capturing about two-thirds of the total exfoliation energy obtained with C_6, C_8, and C_{10} terms. Scaling the C_6 dispersion energy by the same factor optimized for the KB49 set of molecular dimers instead results in overbinding. Also, this scaling gives incorrect long-range behaviour of the dispersion energy, with too much stabilization over the entire PES. Inclusion of both C_6 and C_8 terms significantly reduces the underbinding seen with C_6 alone and recovers roughly 95% of the total exfoliation energy. Scaling of the C_8 term again overbinds but to a much smaller extent than in the case of the scaled C_6. Finally, inclusion of C_{10} improves agreement with the QMC reference and its relatively small (5%) contribution supports neglect of even higher order pairwise terms in the XDM dispersion energy.

7 Importance of ATM Terms for Molecular Systems

Next, we assess the impact of atomic many-body (C_9) dispersion terms for the X23 set. As before, we will focus on the leading atomic three-body dispersion contribution, the ATM term. To compute the ATM term for molecular systems, a suitable form for the damping function must be chosen, as this will ultimately affect the relative magnitude of the ATM term at the equilibrium geometries.[64]

Of the several choices of 3-body damping function used previously in the literature,[64] one option is the same Becke-Johnson

damping[80,82] used for the pairwise terms in XDM,

$$f_n^{\mathrm{BJ}}(R) = \frac{R^n}{R^n + R_{\mathrm{vdW}}^n}. \quad (17)$$

Here, $R_{\mathrm{vdW}} = a_1 R_{c,ij} + a_2$, where R_c is a sum of "critical" atomic radii determined from ratios of the dispersion coefficients[80] and a_1 and a_2 are the functional-specific XDM damping parameters. Another option is the Tang-Toennies damping function,[97]

$$f_n^{\mathrm{TT}}(R) = 1 - e^{-bR}\left(\sum_{k=0}^{n}\frac{(bR)^k}{k!}\right), \quad (18)$$

where $b = -a_3 R_{vdW,ij} + a_4$ is a range parameter proportional to the sum of van der Waals radiii, R_{vdW}. In this perspective, we use BJ damping, rather than TT, where the definition of the b exponent (Eqn 18)[98,99] is problematic. The value of this exponent can become negative for some contacts, making the function switch between damping energy contributions to zero or sharply increasing them.

In addition to the type of damping function used, there are various possibilities regarding the construction of the three-body damping product. For the pairwise dispersion terms, the damping is a simple function of the internuclear separation, R_{ij}. However, for a three-body term, the damping function depends on three internuclear distances, R_{ij}, R_{jk}, and R_{ik}. Since the damping function has to be symmetric with respect to the permutation of the indices, the simplest is to use a product of three pairwise damping functions, although a single damping function involving an averaged distance could also be employed, as in the D3 dispersion correction.[23] Three examples, in order of increasing damping, are the product of three f_3 functions,[100]

$$f_9^{(3)} = f_3(R_{ij}) f_3(R_{jk}) f_3(R_{ik}), \quad (19)$$

the product of three $\sqrt{f_6}$ functions,[101]

$$f_9^{(\sqrt{6})} = \sqrt{f_6(R_{ij}) f_6(R_{jk}) f_6(R_{ik})}, \quad (20)$$

and the product of three f_6 functions,[98,99]

$$f_9^{(6)} = f_6(R_{ij}) f_6(R_{jk}) f_6(R_{ik}). \quad (21)$$

In the interest of mathematical simplicity, and for consistency with the pairwise terms, our ATM dispersion energy is computed as

$$E_{\mathrm{ATM}}^{(3)} = s_9 \sum_{i<j<k} \frac{C_{9,ijk}\left[3\cos(\theta_i)\cos(\theta_j)\cos(\theta_k)+1\right] f_9^{\mathrm{BJ}(3)}(R_{ij},R_{jk},R_{ki})}{R_{ij}^3 R_{jk}^3 R_{ki}^3}$$

$$= s_9 \sum_{i<j<k} \frac{C_{9,ijk}\left[3\cos(\theta_i)\cos(\theta_j)\cos(\theta_k)+1\right]}{(R_{ij}^3 + R_{vdW,ij}^3)(R_{jk}^3 + R_{vdW,jk}^3)(R_{ki}^3 + R_{vdW,ki}^3)}, \quad (22)$$

which involves the product of three f_3 BJ damping functions. The s_9 parameter is an empirical scaling factor, analogous to that used for the C_8 term in the D3 model.[23]

We consider the usual XDM dispersion energy, including C_6, C_8, and C_{10} terms, as well as the two XDM variants with empirical scaling of the C_6 or C_8 terms introduced in the previous section. The BJ damping parameters and scale factors shown in Table 3 are retained and a scaled C_9 term added to the dispersion energy, with the s_9 parameter fit to minimize the RMSP error for the X23 set. The results are shown in Table 4.

The X23 set was used for fitting since fits on the KB49 set result in either zeroing of the C_9 term or unphysical negative coefficients with both base functionals and all XDM variants. This occurs because, as seen previously,[98] the ATM dispersion energy is vanishingly small, except for π-stacked dimers, for which it is repulsive. As GGAs, and particularly PBE, tend to underbind π-stacking relative to H-bonding, inclusion of C_9 increases the error, unless negative scaling coefficients are permitted. However, for the X23 set, the results show how the addition of C_9 can improve performance for molecular crystals in some specific cases.

As seen in the previous section, evaluating the dispersion energy using only a scaled C_6 term, which works for molecular dimers, results in severe overbinding for the X23 set due to replacement of the more rapidly decaying C_8 term (Table 3). Hence, addition of the generally repulsive C_9 term can offset this error, resulting in significant reduction of the MAE with both base functionals. Interestingly, the optimum scaling of the C_9 term with PBE is very close to 1, explaining the good results obtained from dispersion models including only C_6 and C_9 terms,[98] but without C_8 or C_{10}. However, once such higher-order pairwise dispersion terms are included, the overbinding of the X23 set is reduced, with a concomitant reduction in the optimum C_9 contribution, again yielding s_9 values that are near zero or unphysically negative to offset errors from the base GGA functional. Similar results to those presented in Table 4 are also obtained if a product of three f_6 BJ damping functions (as in Eqn. 21) is used, with MAEs differing by only 0.02-0.07 kcal/mol.

While ATM terms are important in noble-gas trimers,[100] and can be added to MP2 theory to improve performance for molecular trimers,[99] errors in the base density-functional treatment of such systems are much larger than the ATM dispersion energies.[90,94,102–104] Thus, empirical fitting of these terms serves to either reduce errors from the base density functional (for standard XDM) or from neglect of higher-order terms in the pairwise expansion (for scaled C_6-only XDM).

8 Summary

Returning to the titular question, "many-body" dispersion can refer to two distinct phenomena, both of which cause the dispersion energy to be non-additive (i.e., it cannot be written as a sum of the dispersion energies of all atomic pairs taken in isolation). Electronic many-body effects refer to the change in the pairwise (C_6, C_8, C_{10},...) dispersion coefficients resulting from changing atomic environment. Atomic many-body effects correspond to the non-additivity introduced by three-atom and higher order dispersion energy terms, the leading contribution being the Axilrod-Teller-Muto three-body term, with C_9 dispersion coefficient. Care must be taken to distinguish between these two different phenomena.

Accounting for electronic many-body effects is essential for a good description of intermolecular interactions. These effects are important because the pairwise dispersion coefficients change sig-

Table 4 Optimum ATM term scaling parameter and resulting performance on the X23 benchmarks for various combinations of dispersion-energy terms. An "×" indicates an unscaled term and "s" indicates multiplicative scaling. The BJ damping parameters and C_6 or C_8 scale factors (where applicable) are taken from Table 3. The C_9 term uses BJ damping, as in Eqn 22. All errors are in units of kcal/mol. MAE: mean absolute error; ME: mean error, a negative value indicates underbinding.

Pairwise Terms			C_9 Damping Parameters	X23 MAE	
C_6	C_8	C_{10}	s_9	no ATM	with ATM
PBE-XDM					
s			0.9960	1.65	1.06
×	s		-0.0483	0.89	0.89
×	×	×	-0.6716	1.12	0.87
B86bPBE-XDM					
s			1.1586	1.78	1.02
×	s		0.0961	0.84	0.83
×	×	×	-0.2924	0.86	0.85

nificantly with even small changes in chemical environment, for instance, when van der Waals complexes are formed. Electronic many-body effects are not captured by an atom-typed model (D2), and can only be roughly approximated in a model that depends on coordination numbers (D3) or atomic volumes (TS) only. They can be captured in pairwise models, like XDM, if the dispersion coefficients have a sufficiently sophisticated dependence on the electron density. They are also captured implicitly by non-local correlation functionals designed to account for dispersion interactions.

In contrast, atomic many-body effects are usually negligible. Their dependence may previously have been overestimated based on the ambiguity in the choice of damping function and as a result of empirical parameter fitting. Fitting the damping function parameters or scaling the leading atomic many-body contribution (the Axilrod-Teller-Muto term, ATM) can be used to compensate for errors in the pairwise dispersion energy or in the base density functional. The magnitude of the atomic many-body effects calculated with such dispersion functionals are not physically or chemically meaningful.

Conflicts of interest

There are no conflicts to declare.

Acknowledgements

The authors acknowledge Compute Canada and the MALTA Consolider supercomputing centre for computational resources. We also acknowledge the Natural Sciences and Engineering Research Council of Canada (NSERC) for funding to ERJ and LML, the Walter C. Sumner Foundation for funding to LML, and the Spanish government for funding to AOR (RyC-2016-20301, PGC2018-097520-A-100, and RED2018-102612-T). ERJ also thanks Prof. P.M.W. Gill for the suggestion of the Drude oscillator and Prof. C.N. Rowley for helpful discussions.

:

Notes and references

1 F. London, *Z. Physik*, 1930, **63**, 245–279.

2 A. Stone, *The Theory of Intermolecular Forces*, Clarendon Press, 1997.

3 K. Autumn, M. Sitti, Y. A. Liang, A. M. Peattie, W. R. Hansen, S. Sponberg, T. W. Kenny, R. Fearing, J. N. Israelachvili and R. J. Full, *Proc. Natl. Acad. Sci.*, 2002, **99**, 12252âĂŞ12256.

4 M. Lessel, P. Loskill, F. Hausen, N. N. Gosvami, R. Bennewitz and K. Jacobs, *Phys. Rev. Lett.*, 2013, **111**, 035502.

5 W. Liu, A. Tkatchenko and M. Scheffler, *Acc. Chem. Res.*, 2014, **47**, 3369–3377.

6 M. Micoulaut, A. Piarristeguy, H. Flores-Ruiz and A. Pradel, *Phys. Rev. B*, 2017, **96**, 184204.

7 T. Risthaus and S. Grimme, *J. Chem. Theory Comput.*, 2013, **9**, 1580–1591.

8 J. Moellmann and S. Grimme, *Phys. Chem. Chem. Phys.*, 2010, **12**, 8500–8504.

9 M. Kolář, T. Kubař and P. Hobza, *J. Phys. Chem. B*, 2011, **115**, 8038–8046.

10 W. Kohn and L. J. Sham, *Phys. Rev.*, 1965, **140**, 1133.

11 K. Burke, *J. Chem. Phys.*, 2012, **136**, 150901.

12 A. D. Becke, *J. Chem. Phys.*, 2014, **140**, 18A301.

13 J. Klimeš and A. Michaelides, *J. Chem. Phys.*, 2012, **137**, 120901.

14 S. Grimme, A. Hansen, J. G. Brandenburg and C. Bannwarth, *Chem. Rev.*, 2016, **116**, 5105–5154.

15 J. Hermann, R. A. DiStasio Jr. and A. Tkatchenko, *Chem. Rev.*, 2017, **117**, 4714–4758.

16 *Non-covalent Interactions in Quantum Chemistry and Physics*, ed. A. Otero-de-la-Roza and G. DiLabio, Elsevier, 2017.

17 Y. Andersson, D. C. Langreth and B. I. Lundqvist, *Phys. Rev. Lett.*, 1996, **76**, 102–105.

18 T. Sato, T. Tsuneda and K. Hirao, *Mol. Phys.*, 2005, **103**, 1151–1164.

19 M. Dion, H. Rydberg, E. Schröder, D. C. Langreth and B. I. Lundqvist, *Phys. Rev. Lett.*, 2004, **92**, 246401.

20 K. Lee, É. D. Murray, L. Kong, B. I. Lundqvist and D. C. Langreth, *Phys. Rev. B*, 2010, **82**, 081101.

21 E. Schröder, V. R. Cooper, K. Berland, B. I. Lundqvist, P. Hyldgaard and T. Thonhauser, *Non-covalent Interactions in Quantum Chemistry and Physics*, Elsevier, 2017, ch. 8, pp. 241–274.

22 S. Grimme, *J. Comput. Chem.*, 2006, **27**, 1787–1799.

23 S. Grimme, J. Antony, S. Ehrlich and H. Krieg, *J. Chem. Phys.*, 2010, **132**, 154104.

24 E. Caldeweyher, S. Ehlert, A. Hansen, H. Neugebauer, S. Spicher, C. Bannwarth and S. Grimme, *J. Chem. Phys.*, 2019, **150**, 154122.

25 A. Tkatchenko and M. Scheffler, *Phys. Rev. Lett.*, 2009, **102**, 073005.

26 A. Tkatchenko, R. A. DiStasio, R. Car and M. Scheffler, *Phys. Rev. Lett.*, 2012, **108**, 236402.

27 A. D. Becke and E. R. Johnson, *J. Chem. Phys.*, 2007, **127**, 154108.

28 E. R. Johnson, *Non-covalent Interactions in Quantum Chemistry and Physics*, Elsevier, 2017, ch. 5, pp. 169–194.

29 A. M. Reilly and A. Tkatchenko, *J. Chem. Phys.*, 2013, **139**, 024705.

30 W. Ouyang, I. Azuri, D. Mandelli, A. Tkatchenko, L. Kronik, M. Urbakh and O. Hod, *J. Chem. Theory Comput.*, 2020, **16**, 666–676.

31 F. Maass, M. Ajdari, F. C. Kabeer, M. Vogtland, A. Tkatchenko and P. Tegeder, *J. Phys. Chem. Lett.*, 2019, **10**, 1000–1004.

32 M. Stöhr and A. Tkatchenko, *Science Adv.*, 2019, **5**, eaax0024.

33 A. Dalgarno and W. D. Davison, *Adv. At. Mol. Phys.*, 1966, **2**, 1–32.

34 B. M. Axilrod and E. Teller, *J. Chem. Phys.*, 1943, **11**, 299–300.

35 Y. Muto, *J. Phys. Math. Soc. Japan*, 1943, **17**, 629.

36 J. F. Dobson, *Int. J. Quantum Chem.*, 2014, **114**, 1157–1161.

37 K. Vanommeslaeghe, E. Hatcher, C. Acharya, S. Kundu, S. Zhong, J. Shim, E. Darian, O. Guvench, P. Lopes, I. Vorobyov and A. D. MacKerell Jr., *J. Comput. Chem.*, 2010, **31**, 671âĂŞ690.

38 J. Wang, R. M. Wolf, J. W. Caldwell, P. A. Kollman and D. A. Case, *J. Comput. Chem.*, 2004, **25**, 1157âĂŞ1174.

39 W. L. Jorgensen and J. Tirado-Rives, *Proc. Natl. Acad. Sci.*, 2005, **102**, 6665–6670.

40 R. Ahlrichs, R. Penco and G. Scoles, *Chem. Phys.*, 1977, **19**, 119–130.

41 M. Elstner, P. Hobza, T. Frauenheim, S. Suhai and E. Kaxiras, *J. Chem. Phys.*, 2001, **114**, 5149–5155.

42 X. Wu, M. C. Vargas, S. Nayak, V. Lotrich and G. Scoles, *J. Chem. Phys.*, 2001, **115**, 8748–8757.

43 Q. Wu and W. Yang, *J. Chem. Phys.*, 2002, **116**, 515.

44 T. Brinck, J. S. Murray and P. Politzer, *J. Chem. Phys.*, 1993, **98**, 4305–4306.

45 A. D. Becke and E. R. Johnson, *J. Chem. Phys.*, 2006, **124**, 014104.

46 F. O. Kannemann and A. D. Becke, *J. Chem. Phys.*, 2012, **136**, 034109.

47 A. Otero-de-la-Roza and E. R. Johnson, *J. Chem. Phys.*, 2012, **136**, 174109.

48 A. Otero-de-la-Roza and E. R. Johnson, *J. Chem. Phys.*, 2013, **138**, 204109.

49 A. Otero-de-la-Roza, J. D. Mallory and E. R. Johnson, *J. Chem. Phys.*, 2014, **140**, 18A504.

50 A. Otero-de-la-Roza, E. R. Johnson and G. A. DiLabio, *J. Chem. Theory Comput.*, 2014, **10**, 5436–5447.

51 A. Otero-de-la-Roza and E. R. Johnson, *J. Chem. Phys.*, 2012, **137**, 054103.

52 A. Otero-de-la-Roza, B. H. Cao, I. K. Price, J. E. Hein and E. R. Johnson, *Angew. Chem. Int. Ed.*, 2014, **53**, 7879–7882.

53 S. R. Whittleton, A. Otero-de-la-Roza and E. R. Johnson, *J. Chem. Theory Comput.*, 2017, **13**, 441–450.

54 S. R. Whittleton, A. Otero-de-la-Roza and E. R. Johnson, *J. Chem. Theory Comput.*, 2017, **13**, 5332–5342.

55 A. Otero-de-la-Roza, L. M. LeBlanc and E. R. Johnson, *J. Chem. Theory Comput.*, 2019, **15**, 4933–4944.

56 M. S. Christian, A. Otero-de-la-Roza and E. R. Johnson, *J. Chem. Theory. Comput.*, 2016, **12**, 3305–3315.

57 M. S. Christian, A. Otero-de-la-Roza and E. R. Johnson, *Carbon*, 2017, **118**, 184–191.

58 M. S. Christian, A. Otero-de-la-Roza and E. R. Johnson, *Carbon*, 2017, **124**, 531–540.

59 A. Otero-de-la-Roza, L. M. LeBlanc and E. R. Johnson, *J. Phys. Chem. Lett.*, 2020, **11**, 2298–2302.

60 E. R. Johnson, *J. Chem. Phys.*, 2011, **135**, 234109.

61 M. Mohebifar, E. R. Johnson and C. N. Rowley, *J. Chem. Theory Comput.*, 2017, **13**, 6146–6157.

62 E. Walters, M. Mohebifar, E. R. Johnson and C. N. Rowley, *J. Phys. Chem. B*, 2018, **122**, 6690–6701.

63 F. L. Hirshfeld, *Theor. Chim. Acta*, 1977, **44**, 129–138.

64 A. Otero-de-la-Roza and E. R. Johnson, *J. Chem. Phys.*, 2013, **138**, 054103.

65 A. D. Becke and M. R. Roussel, *Phys. Rev. A*, 1989, **39**, 3761–3767.

66 A. D. Becke and E. R. Johnson, *J. Chem. Phys.*, 2005, **123**, 154101.

67 A. D. Becke, *J. Chem. Phys.*, 2003, **119**, 2972–2977.

68 W. Kauzmann, *Quantum Chemistry*, Academic Press Inc., 1957, pp. 507–509.

69 M. J. Frisch, G. W. Trucks, H. B. Schlegel, G. E. Scuseria, M. A. Robb, J. R. Cheeseman, G. Scalmani, V. Barone, B. Mennucci, G. A. Petersson, H. Nakatsuji, M. Caricato, X. Li, H. P. Hratchian, A. F. Izmaylov, J. Bloino, G. Zheng, J. L. Sonnenberg, M. Hada, M. Ehara, K. Toyota, R. Fukuda, J. Hasegawa, M. Ishida, T. Nakajima, Y. Honda, O. Kitao, H. Nakai, T. Vreven, J. A. Montgomery, Jr., J. E. Peralta, F. Ogliaro, M. Bearpark, J. J. Heyd, E. Brothers, K. N. Kudin, V. N. Staroverov, R. Kobayashi, J. Normand, K. Raghavachari, A. Rendell, J. C. Burant, S. S. Iyengar, J. Tomasi, M. Cossi, N. Rega, J. M. Millam, M. Klene, J. E. Knox, J. B. Cross, V. Bakken, C. Adamo, J. Jaramillo, R. Gomperts, R. E. Stratmann, O. Yazyev, A. J. Austin, R. Cammi, C. Pomelli, J. W. Ochterski, R. L. Martin, K. Morokuma, V. G. Zakrzewski, G. A. Voth, P. Salvador, J. J. Dannenberg, S. Dapprich, A. D. Daniels, O. Farkas, J. B. Foresman, J. V. Ortiz, J. Cioslowski and D. J. Fox, *Gaussian 09 Revision B.1*, Gaussian Inc. Wallingford CT 2009.

70 2020, The postg program is available from http://schooner.chem.dal.ca.

71 C. Adamo and V. Barone, *J. Chem. Phys.*, 1999, **110**, 6158–6170.

72 2020, The canoical XDM coefficients for this and other functionals can be found at http://schooner.chem.dal.ca.

73 *NIST chemistry webbook, NIST Standard Reference Database Number 69*, ed. P. J. Linstrom and W. G. Mallard, National Institute of Standards and Technology Washington, Gaithersburg MD, 20899, 2019.

74 G. Scalmani and M. J. Frisch, *J. Chem. Phys.*, 2010, **132**, 114110.

75 A. J. Cohen, P. Mori-Sánchez and W. Yang, *Science*, 2008, **321**, 792–794.

76 M.-C. Kim, E. Sim and K. Burke, *Phys. Rev. Lett.*, 2013, **111**, 073003.

77 M.-C. Kim, E. Sim and K. Burke, *J. Chem. Phys.*, 2014, **140**, 18A528.

78 A. Wasserman, J. Nafziger, K. Jiang, M.-C. Kim, E. Sim and K. Burke, *Ann. Rev. Phys. Chem.*, 2017, **68**, 555–581.

79 J. Perdew, K. Burke and M. Ernzerhof, *Phys. Rev. Lett.*, 1996, **77**, 3865–3868.

80 E. R. Johnson and A. D. Becke, *J. Chem. Phys.*, 2006, **124**, 174104.

81 M. Alkan, P. Xu and M. S. Gordon, *J. Phys. Chem. A*, 2019, **123**, 8406–8416.

82 S. Grimme, S. Ehrlich and L. Goerigk, *J. Comput. Chem.*, 2011, **32**, 1456–1465.

83 F. O. Kannemann and A. D. Becke, *J. Chem. Theory Comput.*, 2010, **6**, 1081–1088.

84 P. E. Blöchl, *Phys. Rev. B*, 1994, **50**, 17953.

85 P. Giannozzi, S. Baroni, N. Bonini, M. Calandra, R. Car, C. Cavazzoni, D. Ceresoli, G. Chiarotti, M. Cococcioni, I. Dabo, A. Dal Corso, S. Fabris, G. Fratesi, S. de Gironcoli, R. Gebauer, U. Gerstmann, C. Gougoussis, A. Kokalj, M. Lazzeri, L. Martin-Samos, N. Marzari, F. Mauri, R. Mazzarello, S. Paolini, A. Pasquarello, L. Paulatto, C. Sbraccia, S. Scandolo, G. Sclauzero, A. P. Seitsonen, A. Smogunov, P. Umari and R. M. Wentzcovitch, *J. Phys.: Condens. Matter*, 2017, **29**, 465901.

86 A. D. Becke, *J. Chem. Phys.*, 1986, **85**, 7184.

87 D. J. Lacks and R. G. Gordon, *Phys. Rev. A*, 1993, **47**, 4681.

88 Y. Zhang, W. Pan and W. Yang, *J. Chem. Phys.*, 1997, **107**, 7921–7925.

89 F. O. Kannemann and A. D. Becke, *J. Chem. Theory Comput.*, 2009, **5**, 719–727.

90 M. J. Gillan, *J. Chem. Phys.*, 2014, **141**, 224106.

91 With version 6.3 of Quantum ESPRESSO,[85] the optimum XDM parameters and KB49 statistics are very similar, but not exactly equal, to those reported in previous work.[28,55].

92 A. Otero-de-la-Roza and E. R. Johnson, *J. Chem. Theory Comput.*, 2015, **11**, 4033–4040.

93 M. J. Gillan, D. Alfè and A. Michaelides, *J. Chem. Phys.*, 2016, **144**, 130901.

94 A. Otero-de-la-Roza, G. A. DiLabio and E. R. Johnson, *J. Chem. Theory Comput.*, 2016, **12**, 3160–3175.

95 J. Moellmann and S. Grimme, *J. Phys. Chem. C*, 2014, **118**, 7615–7621.

96 L. Spanu, S. Sorella and G. Galli, *Phys. Rev. Lett.*, 2009, **103**, 196401.

97 K. Tang and J. P. Toennies, *J. Chem. Phys.*, 1984, **80**, 3726–3741.

98 O. A. von Lilienfeld and A. Tkatchenko, *J. Chem. Phys.*, 2010, **132**, 234109.

99 Y. H. Huang and G. J. O. Beran, *J. Chem. Phys.*, 2015, **143**, 044113.

100 W. Cencek, K. Patkowski and K. Szalewicz, *J. Chem. Phys.*, 2009, **131**, 064105.

101 M. Cvitaš, P. Soldan and J. Hutson, *Mol. Phys.*, 2006, **104**, 23–31.

102 W. Jankiewicz, R. Podeszwa and H. A. Witek, *J. Chem. Theory Comput.*, 2018, **14**, 5079–5089.

103 J. Řezáč, Y. Huang, P. Hobza and G. J. O. Beran, *J. Chem. Theory Comput.*, 2015, **11**, 3065–3079.

104 A. Tkatchenko and O. A. von Lilienfeld, *Phys. Rev. B*, 2008, **78**, 045116.